

# Fabrication of Sub-10 nm Metallic Lines of Low Line-Width Roughness by Hydrogen Reduction of Patterned Metal–Organic Materials

By Mihaela Nedelcu, Mohammad S. M. Saifullah,\* David G. Hasko, Arang Jang, David Anderson, Wilhelm T. S. Huck, Geraint A. C. Jones, Mark E. Welland, Dae Joon Kang,\* and Ullrich Steiner\*

To Professor Seshadri Seetharaman, for his contribution to extractive metallurgy

The fabrication of very narrow metal lines by the lift-off technique, especially below sub-10 nm, is challenging due to thinner resist requirements in order to achieve the lithographic resolution. At such small length scales, when the grain size becomes comparable with the line-width, the built-in stress in the metal film can cause a break to occur at a grain boundary. Moreover, the line-width roughness (LWR) from the patterned resist can result in deposited metal lines with a very high LWR, leading to an adverse change in device characteristics. Here a new approach that is not based on the lift-off technique but rather on low temperature hydrogen reduction of electron-beam patterned metal naphthenates is demonstrated. This not only enables the fabrication of sub-10 nm metal lines of good integrity, but also of low LWR, below the limit of 3.2 nm discussed in the *International Technology Roadmap for Semiconductors*. Using this method, sub-10 nm nickel wires are obtained by reducing patterned nickel naphthenate lines in a hydrogen-rich atmosphere at 500 °C for 1 h. The LWR (i.e.,  $3 \sigma_{\text{LWR}}$ ) of these nickel nanolines was found to be 2.9 nm. The technique is general and is likely to be suitable for fabrication of nanostructures of most commonly used metals (and their alloys), such as iron, cobalt, nickel, copper, tungsten, molybdenum, and so on, from their respective metal–organic compounds.

## 1. Introduction

The fabrication of very narrow and high density metal lines is a key enabling technology in the areas of microelectronics and physics.<sup>[1]</sup> Usually, such narrow lines are formed by separate lithographic and pattern transfer processes. This approach fails, however, when the line-width is reduced significantly below 10 nm.<sup>[2]</sup> In order to fabricate lines of this size, very thin resist layers must be used in order to achieve the required lithographic resolution. But the pattern transfer process (either lift-off or etching) becomes increasingly difficult as the resist thickness is reduced. Finally, the properties of the deposited metal film used to form the wire can lead to failure if the grain size is comparable with the line-width and the built-in stress in the metal film causes a break to occur at a grain boundary.<sup>[3]</sup>

[\*] Dr. M. S. M. Saifullah  
Patterning and Fabrication Capability Group, Institute of Materials Research and Engineering, A\*STAR (Agency for Science, Technology and Research)  
3 Research Link, Singapore 117602 (Republic of Singapore)  
E-mail: saifullahm@imre.a-star.edu.sg  
Prof. D. J. Kang, A. Jang  
BK 21 Physics Research Division, Department of Energy Science, Institute of Basic Sciences, SKKU Advanced Institute of Nanotechnology, Sungkyunkwan University  
300 Cheoncheon-Dong, Jangan-Gu, Suwon 440-746 (South Korea)  
E-mail: dj kang@skku.edu  
Prof. U. Steiner, Dr. M. Nedelcu,<sup>+</sup> D. Anderson,<sup>‡</sup> Dr. G. A. C. Jones  
Department of Physics, University of Cambridge  
Madingley Road, Cambridge CB3 0HE (United Kingdom)  
E-mail: us222@phy.cam.ac.uk

Prof. U. Steiner, Dr. D. G. Hasko,<sup>†</sup> Prof. W. T. S. Huck,  
Prof. M. E. Welland  
The Nanoscience Centre, University of Cambridge  
11 J. J. Thomson Avenue, Cambridge CB3 0FF (United Kingdom)

Prof. U. Steiner  
Freiburg Institute of Advanced Studies (FRIAS)  
Albert-Ludwigs-Universität Freiburg  
Albertstraße 19, D-79104 Freiburg i.Br. (Germany)

Prof. W. T. S. Huck  
Melville Laboratory, Department of Chemistry, University of Cambridge  
Lensfield Road, Cambridge CB2 1EW (United Kingdom)

<sup>[+]</sup>Current address: Department of Chemistry and Biochemistry, Ludwig-Maximilians-Universität München, Butenandstr. 11 (Building E), München (Germany)

<sup>[‡]</sup>Current address: School of Physics, University of Exeter, Stocker Road, Exeter EX4 4QL (United Kingdom)

<sup>[†]</sup>Current address: Centre for Advanced Electronics and Photonics (CAPE), University of Cambridge, 9 J. J. Thomson Avenue, Cambridge CB3 0FA (United Kingdom)

DOI: 10.1002/adfm.201000219

Apart from the traditional lift-off technique, other less commonly used methods to deposit nanostructures of metals are electron-beam-induced deposition (EBID)<sup>[4]</sup> and ion-beam-induced deposition (IBID). EBID offers a resolution close to ~3 nm but the results appear to be confined to dots only.<sup>[5,6]</sup> Moreover, it suffers from several drawbacks, for example, impurities resulting from the incorporation of carbon and oxygen from the metal–organic precursor due to its incomplete dissociation. Often a post-treatment procedure is applied to remove the impurities and improve the relative metal content. On the other hand, IBID is carried out in the focused gallium ion beam microscopes (FIB).<sup>[7]</sup> Due to the combined effects of the larger cross section for dissociation by ions, the higher mass of ions resulting in more component decomposition per reaction and possible beam-induced local heating, the deposits in the case of IBID tend to be of higher purity. With IBID, the principal drawbacks are gallium implantation from the ion beam, top surface damage and a poor resolution with larger tails. Due to the above mentioned reasons, both EBID and IBID have not yet been fully embraced as nanotechnology solutions.

Direct-write electron-beam nanolithography is now a well-established technique for fabricating nanostructures *without* the lift-off step. Increasingly, it is used to pattern metal<sup>[8]</sup> and oxides<sup>[9–12]</sup> from metal–organic precursors at high resolutions. In a recent study, 30-nm-wide palladium lines were obtained by direct patterning of palladium alkanethiolate by electrons and its subsequent reduction to palladium metal by heating it in air.<sup>[8]</sup> In this work, we report on an alternative strategy of using hydrogen reduction of an electron beam-exposed metal naphthenate resist film to form patterned metal lines of good integrity at the sub-10 nm size scale. Although the reduction of metal oxides to the base metals (such as Ni, Co, Fe, Cu, Mo, and W) using hydrogen is well known,<sup>[13–18]</sup> there have been no attempts to use this process in the fabrication of metal nanostructures. It has previously been observed, in studies of oxide-hydrogen reaction kinetics, that nanometer-scale-grained pure metal and alloy films can be produced successfully.<sup>[13]</sup> The reduction of metal oxides to their respective metals by hydrogen is best understood by studying the principles of extractive metallurgy, and in particular, the Ellingham diagram of oxides.<sup>[19]</sup> The Ellingham diagram shows the plot of the free energy change that occurs with a change in temperature when 1 g molecule of a common reactant (O<sub>2</sub> in our case) is used by an element. For the metal oxides that reside *above* the water formation line (i.e., H<sub>2</sub> + 1/2O<sub>2</sub> = H<sub>2</sub>O line), the Ellingham diagram suggests that they are amenable to reduction to their respective metals by hydrogen. In other words, the metal oxides such as NiO, CuO, PbO, CoO, and so on, which are thermodynamically *less* stable than water, can be reduced by hydrogen to their respective metals.

Resists based on metal naphthenates can be patterned by electron-beam exposure and solvent development. The remaining resist can then be reduced to the metal constituents by reduction in a hydrogen-rich atmosphere. This process leads to a small grain size that can be comparable to the line-width, causing only little stress in the metal wire, allowing very small line-widths to be realized (<9 nm) with a low line-width roughness (LWR). In the present study, we investigate the application of this process to pattern nickel nanostructures from its naphthenate. This process is likely to be applicable to a host of other metal–organic materials

and their mixtures that can be reduced to their respective metal and alloys.

## 2. Results and Discussion

The ultimate resolution in electron-beam lithography depends upon various factors. Lower molecular weight resists in combination with a suitable solvent developer system give very high resolution.<sup>[2]</sup> Low-molecular-weight self-developing inorganic resists, mainly consisting of oxides and fluorides, were also tested due to their inherently high resolution capability (~1 nm)

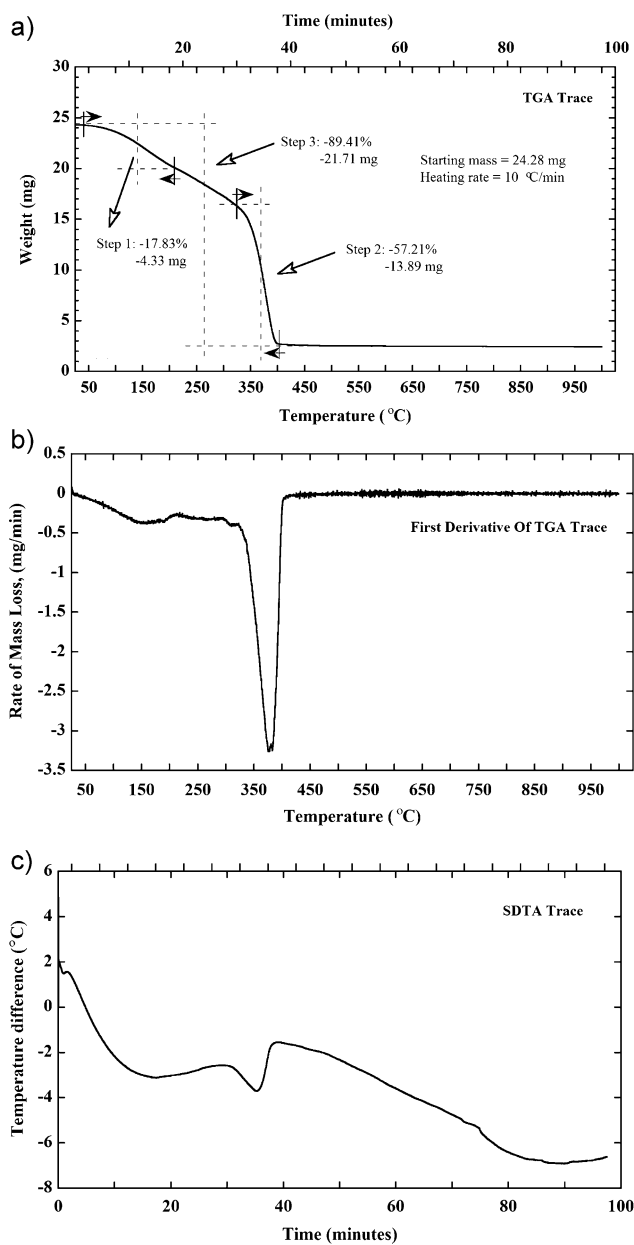


**Figure 1.** a) TGA, b) its first derivative, and c) SDTA analysis of the as-received nickel naphthenate resist. The SDTA trace shows both the temperature and time axes.

but they suffered from very steep dose requirements and were consequently abandoned.<sup>[20]</sup> The forward and backward scattering of electrons during an exposure gives rise to the proximity effect, which has an effect on the achievable ultimate resolution. The forward scattered electrons give rise to a broadening of the beam as it penetrates the resist whereas backward scattered electrons from the substrate give rise to an exposure halo of a radius much greater than the beam diameter. Increasing the accelerating voltage of the instrument and decreasing the resist thickness can reduce the forward scattering component of the proximity effect. On the other hand, backward scattered electrons can be reduced by using a membrane as the substrate. However, the use of a membrane is often impractical when making useful and rugged device structures.

Metal naphthenates are stable and viscous liquids at room temperature allowing the deposition of thin films using conventional resist application techniques. The molecular structure of naphthenates contains cyclopentanes or cyclohexanes, methylene chains  $[-(\text{CH}_2)-]$ , carboxylates and metals. It is typically represented by  $[(\text{cyclopentane})-(\text{CH}_2)_n-\text{COO}]^{-m}-\text{M}^{m+}$ , where M is a metal atom and  $m$  and  $n$  represent the oxidation state of metal and number of  $-\text{CH}_2-$  groups in the molecule, respectively. The low molecular weight of a metal naphthenate molecule, compared to other candidate resist materials, offers the possibility of very high resolution patterning.

The pyrolysis behavior and lithographic characteristics of the metal naphthenates appear not to depend on the nature of the metal atom. The pyrolysis behavior of nickel naphthenate was investigated by thermogravimetric analysis (TGA) and by simultaneous differential thermal analysis (SDTA) in an argon gas atmosphere (Fig. 1). In the 100–200 °C temperature range there was a loss of solvent, primarily toluene, and in the 300–400 °C range, there was a major mass loss (~57%) of organic material. A dip in the higher temperature range data suggests a significant rearrangement of chemical bonds (Fig. 1c), perhaps even crystallization during the formation of an oxide. This data was used as a guide for the processing conditions required to convert nickel naphthenate films into metallic nickel. The reduction reaction was carried out in a hydrogen/argon (60:40) gas atmosphere at 500 °C for 1 h in a tube furnace heated and cooled at the rate of 10 °C min<sup>-1</sup>. Nickel films produced in this way are uniform and continuous (Fig. 2a), with a preferred [100] direction perpendicular to the film (Fig. 2b). Energy dispersive X-ray analysis (EDX) analysis of the film shows presence of nickel and a trace amount of carbon but no oxygen could be

detected. Furthermore, these films demonstrate ferromagnetic properties that are comparable to bulk nickel (Fig. 2c–f).

Figure 3 shows the lithographic behavior of the nickel naphthenate resist after exposure to 100 kV electrons, followed by development in toluene. The sensitivity is  $\sim 9 \text{ mC cm}^{-2}$  (at half the normalized thickness,  $D_{0.5}$ ) and the contrast is  $\gamma \approx 1.4$ . Infrared absorption studies of naphthenate materials by Kakimi et al. suggest that electron beam exposure results in the creation of bridges at the  $-\text{C}=\text{O}$  and/or  $-(\text{CH}_2)_n-$  sites, thereby causing crosslinking and the negative tone behavior.<sup>[21]</sup> These properties

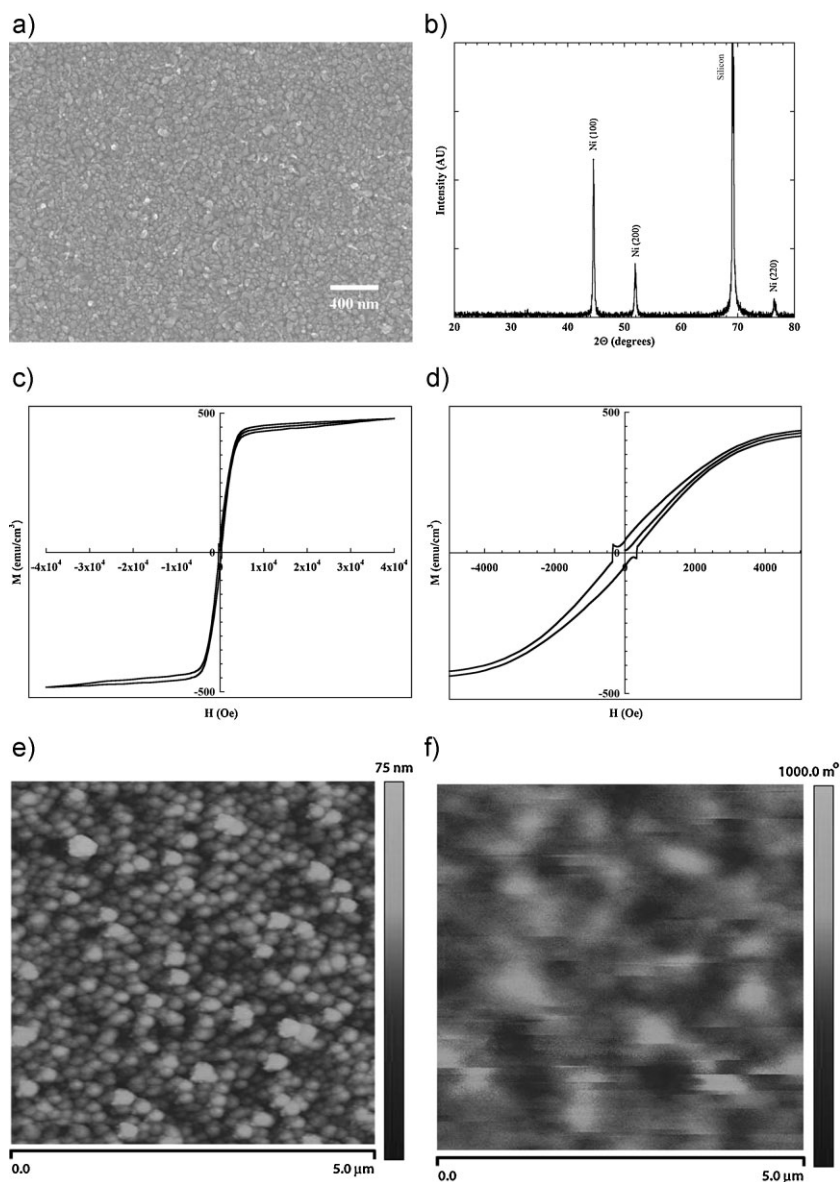


**Figure 2.** Analytical data of a 90–100-nm-thick nickel film obtained after heat-treatment of a nickel naphthenate film at 500 °C for 1 h in a hydrogen/argon (60:40) atmosphere. a) SEM image showing the nanometer-grain morphology of the film. The grain size is  $\sim 100 \text{ nm}$ . b) The X-ray diffraction data of the film appears to have a preferred orientation along [100] direction, which is normal to the film plane. c) Magnetization curve of a 90-nm-thick nickel film, with the hysteresis loop showing its coercivity. d) Magnification of the central part of the curve in (c). e) MFM image of film showing the topography (e) and magnetic contrast (f).

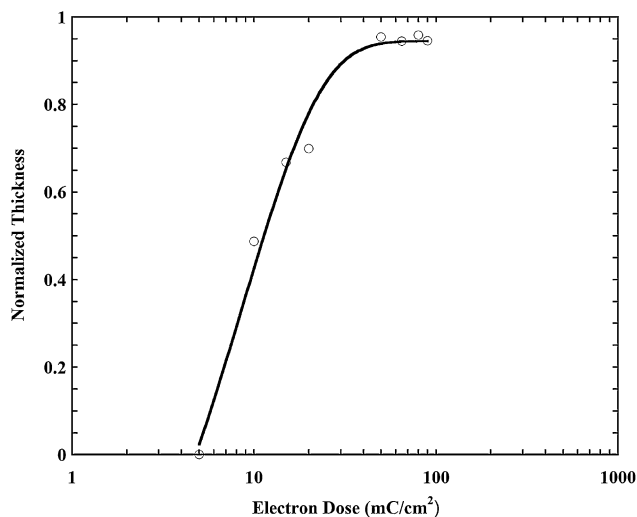


**Figure 3.** Electron-beam exposure response curve of nickel naphthenate resist.

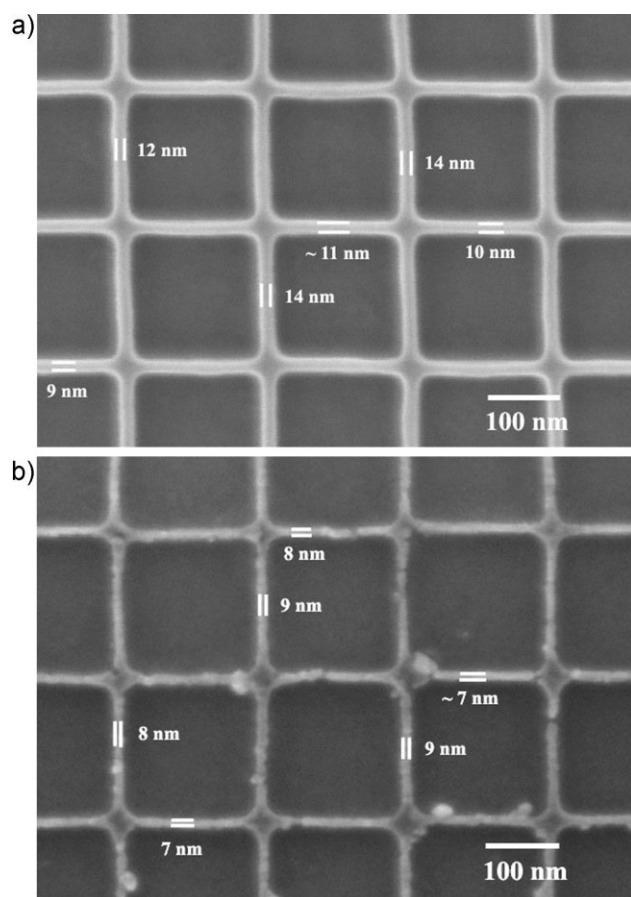


**Figure 4.** SEM images of a) the patterned naphthenate resist,  $\sim 12$ -nm line-widths of nickel naphthenate in the center of the 500- $\mu\text{m}$  main deflection field. b) Reduction of line-width of nickel lines to sub-10 nm sizes after heat-treatment at 500 °C for 1 h in a hydrogen-rich atmosphere.

are suitable for the creation of design patterns, with the nickel naphthenate acting as a negative resist. Figure 4a shows a scanning electron microscopy (SEM) image from the center of a grid array pattern covering a square area with a side length of 500  $\mu\text{m}$  after exposure to an electron dose of  $\sim 300 \text{ mC cm}^{-2}$ . It is worth noting that the line-widths along the  $x$ -direction ( $\sim 10 \text{ nm}$ ) are slightly smaller than those along the  $y$ -direction ( $\sim 13 \text{ nm}$ ), with an aspect ratio (height/width of the line) between  $\sim 7$  and  $\sim 8$  seen across the entire main deflection field (see Supporting Information). Such a difference in the line-widths could be due to a minor offset in the stigmator correction from the optimum value in the  $y$ -direction resulting in slight broadening of the beam in this direction, thereby giving rise to wider line patterns. Patterned metal naphthenates exhibit such high aspect ratios probably because of the strength of the crosslinks formed during electron exposure.<sup>[11]</sup> The grid pattern acts as a support network to maintain the integrity of the structure;<sup>[22]</sup> isolated lines require a higher dose to avoid collapse during the development stage.<sup>[23]</sup>

Patterned structures were heated to 500 °C for 1 h in a hydrogen/argon (60:40) gas atmosphere, leading to shrinkage of the wire section as the organic component is driven off and the residue is reduced to crystalline nickel (Fig. 4b). The line-width after this treatment was  $\sim 7 \text{ nm}$  and  $\sim 9 \text{ nm}$  in  $x$ - and  $y$ -directions, respectively, with presumably comparable grain sizes. Some signs of the Ostwald ripening were visible at the junctions between gridlines of the nickel wires as well as the appearance of grain growth along a few lines. This was not observed for the copper wires of  $\sim 4 \text{ nm}$  line-width prepared by the similar process of hydrogen reduction (see Supporting Information). Another noticeable observation is the high aspect ratios ( $\geq 7$ ) of nickel and copper nanolines without resulting in their deformation or collapse. The reason for this is could be two-fold. First, from the Hall–Petch relationship, it is well-known that the yield strength of the metals increases with decreasing grain size.<sup>[24]</sup> This is due to the fact that the stress needed to actuate a dislocation source is rather high in a nanometer-sized grain. However, for sub-10 nm grain-sized nickel films, there is an evidence of breakdown of the Hall–Petch relationship due to grain boundary–mediated deformation processes,<sup>[25,26]</sup> but the magnitude of breakdown is small enough with little effect on the yield strength of the metal nanostructures. Second, after the heat-treatment the lines were cooled at the rate of  $10 \text{ }^\circ\text{C min}^{-1}$  to avoid building-up of any thermal stresses that may lead to deformation of the nanolines. A combination of high yield strength of the nickel nanostructures and slow cooling to avoid building-up of thermal stresses may have also given them sufficient mechanical durability to withstand the rigors of post-processing such as spin-coating of resist for patterning contact pads. Magnetic force microscopy (MFM) measurement of the sub-10 nm nickel lines did not show any magnetic behavior. The reason for this is unclear, but the lack of a detectable hysteresis loop may be due to small grain size, presumably of the order of the line-width, thus giving rise to decreased crystallinity and increased disorder in the nickel nanoline, resulting in the insufficient sensitivity of the measurement.<sup>[27]</sup>

The LWR quantitatively describes line-width variation. Table 1 compares the LWRs obtained for the nanoline patterns of nickel naphthenate and nickel metal obtained after reduction. Patterned nickel naphthenate lines (mean widths,  $\bar{x} = 10.6 \text{ nm}$ ,  $\bar{y} = 13.1 \text{ nm}$ )

**Table 1.** Line-width, aspects ratio, LWR, and LER obtained for the nickel naphthenate and nickel nanolines along x- and y-directions.

Material	Line-width [nm] (average)	LWR ( $\sigma_{LWR}$ ) [nm]	Pattern height [nm]	Aspect ratio	LWR ( $3 \sigma_{LWR}$ ) [nm]	LER ( $3 \sigma_{LER}$ ) [nm]
Nickel naphthenate	$\bar{x} = 10.6$	$\sigma_{LWR}^x = 0.74$	$\sim 90$	$\sim 8.5$	2.2	1.6
	$\bar{y} = 13.1$	$\sigma_{LWR}^y = 0.73$		$\sim 6.9$	2.2	1.5
Nickel	$\bar{x}_h = 7.6$	$\sigma_{LWR_h}^x = 0.97$	$\sim 60$	$\sim 7.9$	2.9	2.0
	$\bar{y}_h = 8.8$	$\sigma_{LWR_h}^y = 0.99$		$\sim 6.8$	3.0	2.1

show the LWR (standard deviation,  $\sigma_{LWR}$ ) of  $\sigma_{LWR}^x = 0.74$  nm and  $\sigma_{LWR}^y = 0.73$  nm. However, after reduction to nickel, the lines (mean widths,  $\bar{x}_h = 7.6$  nm,  $\bar{y}_h = 8.8$  nm) show a slight increase in the LWR ( $\sigma_{LWR_h}^x = 0.97$  nm and  $\sigma_{LWR_h}^y = 0.99$  nm). The increase in the LWR of the nickel nanolines is most likely due to the formation of a granular nanostructure during the heat-treatment. In the scientific literature, the LWR is usually reported as three standard deviations (i.e.,  $3 \sigma_{LWR}$ ). This would result in  $3 \sigma_{LWR}$  of nickel naphthenate and nickel nanolines of 2.2 and 2.9 nm, respectively. It is interesting to note that the LWR of both nickel naphthenate and nickel nanolines is below the 2009 target of 3.2 nm specified in the *International Technology Roadmap for Semiconductors*.<sup>[28]</sup> Taking into account the 1.47 nm per pixel resolution and other measurement noise in SEM images, the true LWR of the nickel nanolines obtained after the hydrogen reduction is most likely below 2.9 nm.

Assuming no correlation between the right and left edges of the nanolines in the absence of external influences such as defects and topography, the relationship between the LWR and line edge roughness (LER) is given by the equation:<sup>[29]</sup>

$$\sigma_{LWR} = \sqrt{2} \sigma_{LER} \quad (1)$$

Like LWR, the LER is usually reported as three standard deviations (i.e.,  $3 \sigma_{LER}$ ). In our case, the LERs (i.e.,  $3 \sigma_{LER}$ ) of the nickel naphthenate and nickel lines are  $\sim 1.6$  and  $\sim 2.1$  nm, respectively. Recently, Chou and Xia demonstrated that the LER can be improved dramatically by selectively melting of 70-nm-

wide metallic nanostructures for very short periods of time using laser pulses.<sup>[30]</sup> In our case, however, it was the gas-solid reaction, well-below the melting point of nickel, possibly combined with the low initial LER of nickel naphthenate nanolines, that helped in obtaining metallic lines with low LER. Furthermore, the metal lines demonstrate good integrity due to the fact that they were produced at a relatively low temperature of 500 °C and cooled down slowly, which reduces the thermal stresses in the lines.

Four-terminal measurements were used to determine the electrical resistivity ( $\rho$ ) of the nickel nanolines (line-width =  $\sim 42$  nm, height = 30 nm, and length = 164 nm) produced from hydrogen heat-treatment of patterned nickel naphthenate (Fig. 5), yielding a resistivity of  $\sim 9.2 \times 10^{-1} \Omega \text{ cm}$ . On the other hand, the bulk resistivity of nickel is  $\sim 7.12 \times 10^{-6} \Omega \text{ cm}$  at 25 °C.<sup>[31]</sup> A recent study of the electrical resistivity of chemically pure and high quality oriented single crystalline nickel nanowire of 55 nm in diameter using a four-probe method gave a value of  $\sim 1 \times 10^{-5} \Omega \text{ cm}$ .<sup>[32]</sup> Similar values of resistivity were also obtained for highly oriented electrodeposited nickel nanowires of  $\sim 30$  nm in diameter.<sup>[33]</sup> Such a low resistivity was attributed to a very low density in crystallographic defects in the nickel nanowire. The very nature of low-temperature gas–solid type reactions, as epitomized by hydrogen reduction of metal-organics, results in nanograin disordered metals. Given the fact that our  $\sim 42$  nm wide nanocrystalline nickel wires were prepared by hydrogen reduction, enhanced electron scattering from the surface, grain boundaries, and from other defects and residual impurities is expected. Thus the obtained resistivity value for these nickel nanolines (approximately four orders of magnitude above the value for single-crystal nickel nanowire) is therefore not surprising.

### 3. Conclusion

In summary, we have shown that sub-10 nm metal lines of good integrity and low LWR can be obtained by hydrogen reduction of patterned metal naphthenates. This has been made possible by lowering built-in stresses as well as reducing the grain size in the metal nanolines. Fortunately, in addition to nickel and copper, our technique is likely to work for most commonly used metals, such as iron, cobalt, tungsten, molybdenum, and so on, and their alloys, many of which play an important role in the electronic industry. Finally, it is useful to point out the limitations of the use of hydrogen reduction in the fabrication of patterned metallic nanostructures. This method can't be used for metal oxides that reside below the water formation line (i.e. the  $\text{H}_2 + \frac{1}{2}\text{O}_2 = \text{H}_2\text{O}$  line) in the Ellingham diagram. This is because the oxides of these metals are thermodynamically more stable than water, and in some cases are prone to the formation of metal hydrides.

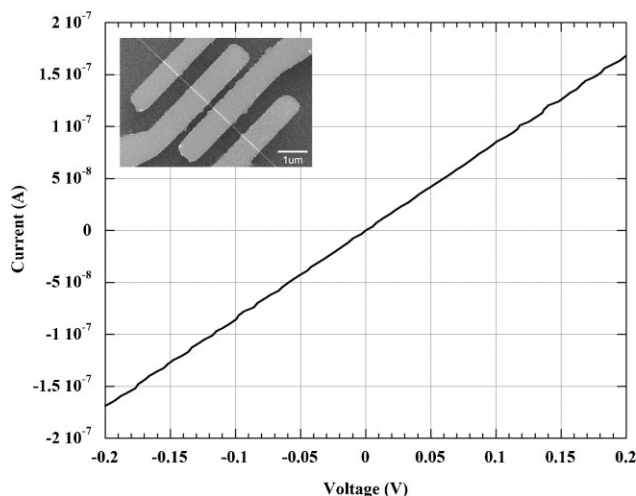


**Figure 5.** Current–voltage ( $I$ – $V$ ) curve of a  $\sim 42$ -nm-wide nickel line obtained using a four-point probe measurement. Inset: Picture of the device assembly.

## 4. Experimental

**Solution Preparation and Patterning:** Silicon wafers were cleaned in acetone, rinsed in iso-propanol and dried with a nitrogen gun. They were then treated in an ozone/oxygen plasma and snow-jetted to ensure removal of organics and dust particles on the surface. Nickel naphthenate (1 mL, Strem Chemicals, ~60% in toluene, 6%–8% Ni) was diluted in toluene (20 mL) and filtered using a 0.2- $\mu\text{m}$  filter. Films with the thicknesses of ~100 nm of nickel naphthenate were prepared by spin-coating onto pre-cleaned silicon wafers at 4000 rpm for 30 s. The solution was filtered using a 0.2- $\mu\text{m}$  filter and spun on pre-cleaned silicon wafers. A Leica VB-6UHR electron beam nanowriter, operating at 100 kV with a probe current of 1.5 nA, was used for high-resolution electron-beam lithography. After the exposure to an electron beam, the resist was developed in toluene for 10 s without rinsing. The topography of the developed pattern was studied using an atomic force microscope (AFM). A LEO 1530VP SEM was used to image high-resolution patterns. It was operated at 5 kV accelerating voltage and the working distance was 3 mm.

**Magnetization Measurements:** A DC SQUID magnetometer was used to investigate the magnetic properties of unpatterned nickel films. The magnetization curve as a function of the applied magnetic field is shown in Figure 2c and d. A magnetic field of  $\pm 4$  Tesla was applied perpendicular to the sample. The measured saturation magnetization ( $M_s$ ) of a 90-nm-thick nickel film was around 430 emu  $\text{cm}^{-3}$ , which is slightly lower compared to bulk nickel of 480 emu  $\text{cm}^{-3}$ . The coercivity of this film was close to 340 Oe (Fig. 2a), which suggests that the film consisted mainly of crystalline nickel. Earlier studies have shown that mixtures of amorphous and crystalline phases have a reduced saturation magnetization and an increased coercivity compared to bulk nickel [27]. In our case, the observed differences between the nickel film and bulk nickel probably arise from disorder in the film, which result from the low processing temperature.

**MFM Measurements:** MFM was used to investigate the magnetic domain structure in a 100-nm-thick nickel film. Figure 2e shows the topographic image, while Figure 2f is the corresponding MFM image showing bright and dark in-plane domain regions.

**Electrical Resistivity:** A four-terminal measurement was used to determine  $\rho$  of the metal film. At room temperature, the sheet resistivity ( $\rho_s$ ) of a 28-nm-thick nickel film was  $9.4 \times 10^{-4} \Omega \text{ cm}$ , which is somewhat lower than the bulk resistivity of nickel ( $\sim 7.12 \times 10^{-6} \Omega \text{ cm}$ ). This indicates that the measured resistivity was increased by the presence of disorder in the nickel, residual impurities or by porosity in the film arising from the hydrogen reduction process.

**Electron-Beam Exposure:** High-resolution nanolithography was performed by writing single-pass lines in a Leica VB-6UHR nanowriter. Across the entire 500- $\mu\text{m}$  square main deflection field, five sets of continuous single pass lines were written in both  $x$ - and  $y$ -directions. These sets were equidistant from each other: two at the edges of the main field, one in the middle, and the last two between the middle and the edges of the main field. In each set there were 10 and 20 single pass lines with 200 and 100 nm pitches, respectively. The beam step size was chosen as 2 nm. A  $10 \times 4$  array of fields was exposed with a start dose of 250 mC  $\text{cm}^{-2}$  and a dose increment of 1.05 per field. This was done in order to find the optimum dose as single pass lines require a considerably higher electron dose compared to large area writing. Each 500- $\mu\text{m}$  pattern field was stepped and settled within 200 ms.

**LWR Measurement:** Digitized SEM images were used to calculate the LWR. The images were acquired at a magnification of 250 000x, with a 1.47 nm per pixel resolution and contained other measurement noise. These images were analyzed using a custom-written program in the SEMPER software. The LWR of the nanolines in  $x$ - and  $y$ -directions was calculated separately, with  $\sim 2 \mu\text{m}$  being the typical line length over which the LWR is averaged.

## Acknowledgements

MSMS would like to thank Dr. C. B. Boothroyd, Center for Electron Nanoscopy, Technical University of Denmark, for his help with the LWR calculations. He also thanks Dr. Eunice Leong and Ms. Siew Lang Teo for

their assistance with electron beam nanolithography. This work was supported by the Ministry of Education, Science and Technology under grants NRF-20090094026 (Priority Research Centers Program), 2009-00591 (KICOS Global Partnership Program) and R31-2008-000-10029-0 (World Class University Program). Partial support by the European network "PolyFilm" under RTN-6 and the IMRE-funded core project no. IMRE/07-1C0304 is gratefully acknowledged. Supporting Information is available online from Wiley InterScience or from the author.

Received: February 3, 2010

Revised: March 26, 2010

Published online: June 18, 2010

- [1] G.-Y. Jung, E. Johnston-Halperin, W. Wu, Z. Yu, S.-Y. Wang, W. M. Tong, Z. Li, J. E. Green, B. A. Sheriff, A. Boukai, Y. Bunimovich, J. R. Heath, R. S. Williams, *Nano Lett.* **2006**, *6*, 351.
- [2] S. Yasin, D. G. Hasko, H. Ahmed, *Appl. Phys. Lett.* **2001**, *78*, 2760.
- [3] R. Koch, *J. Phys.: Condens. Matter* **1994**, *6*, 9519.
- [4] For a recent review of EBID, see A. Botman, J. J. L. Mulders, C. W. Hagen, *Nanotechnology* **2009**, *20*, 372001.
- [5] L. van Kouwen, A. Botman, C. W. Hagen, *Nano Lett.* **2009**, *9*, 2149.
- [6] K. Mitsuishi, M. Shimojo, M. Han, K. Furuya, *Appl. Phys. Lett.* **2003**, *83*, 2064.
- [7] S. Matsui, T. Kaito, J. Fujita, M. Komuro, K. Kanda, Y. Haruyama, *J. Vac. Sci. Technol. B* **2000**, *18*, 3181.
- [8] T. Bhuvana, G. U. Kulkarni, *ACS Nano* **2008**, *2*, 457.
- [9] M. S. M. Saifullah, K. R. V. Subramanian, E. Tapley, D. J. Kang, M. E. Welland, M. Butler, *Nano Lett.* **2003**, *3*, 1587.
- [10] K. R. V. Subramanian, M. S. M. Saifullah, E. Tapley, D. J. Kang, M. E. Welland, M. Butler, *Nanotechnology* **2004**, *15*, 158.
- [11] M. S. M. Saifullah, K. R. V. Subramanian, D. J. Kang, D. Anderson, W. T. S. Huck, G. A. C. Jones, M. E. Welland, *Adv. Mater.* **2005**, *17*, 1757.
- [12] K. Mori, S. Okamura, *Jpn. J. Appl. Phys.* **1992**, *31*, L1143.
- [13] R. Morales, F. J. Tavera, R. E. Aune, S. Seetharaman, *Scand. J. Metall.* **2005**, *34*, 108.
- [14] I. Arvanitidis, A. Kapilashrami, D. Sichen, S. Seetharaman, *J. Mater. Res.* **2000**, *15*, 338.
- [15] U. Tilliander, R. E. Aune, S. Seetharaman, *Metall. Mater. Trans. B* **2006**, *37*, 265.
- [16] L. P. Dorfman, D. L. Houck, M. J. Scheithauer, T. A. Frisk, *J. Mater. Res.* **2002**, *17*, 821.
- [17] J. A. Bustnes, D. Sichen, S. Seetharaman, *Metall. Mater. Trans. B* **1995**, *26*, 547.
- [18] W. V. Schulmeyer, H. M. Ortner, *Int. J. Refract. Met. Hard Mater.* **2002**, *20*, 261.
- [19] *Principles of Extractive Metallurgy*, (Eds: H. S. Ray, A. Ghosh), New Age International (Pr.) Ltd, New Delhi, India **2001**, Ch. 4.
- [20] A recent review on the topic of self-developing inorganic electron beam resists was done by M. S. M. Saifullah, *Cosmos* **2009**, *5*, 1.
- [21] A. Kakimi, S. Okamura, Y. Yagi, K. Mori, T. Tsukamoto, *Jpn. J. Appl. Phys.* **1994**, *33*, 5301.
- [22] M. S. M. Saifullah, K. R. V. Subramanian, D. Anderson, D. J. Kang, W. T. S. Huck, G. A. C. Jones, M. E. Welland, *J. Vac. Sci. Technol. B* **2006**, *24*, 1215.
- [23] S. Okamura, A. Kakimi, Y. Yagi, K. Mori, T. Tsukamoto, in: *ISAF '94 - Proceedings of the Ninth IEEE International Symposium on Applications of Ferroelectrics*, University Park, PA, 7–10 August 1994 (Eds: R. K. Pandey, M. Liu, A. Safari), IEEE, New York **1994**.
- [24] N. Noskova, *J. Phys.: Conf. Ser.* **2008**, *98*, 012027.
- [25] C. A. Schuh, T. G. Nieh, T. Yamasaki, *Scr. Mater.* **2002**, *46*, 735.
- [26] Z. Shan, E. A. Stach, J. M. K. Wiezorek, J. A. Knapp, D. M. Follstaedt, S. X. Mao, *Science* **2004**, *305*, 654.
- [27] J. B. Yi, Y. Z. Zhou, J. Ding, G. M. Chow, Z. L. Dong, T. White, X. Y. Gao, A. T. S. Wee, X. J. Yu, *J. Magn. Magn. Mater.* **2004**, *284*, 303.

- [28] International Technology Roadmap for Semiconductors 2009, Table LITH4A (Resist requirements), [http://www.itrs.net/Links/2009ITRS/2009Chapters\\_2009Tables/2009Tables\\_FOCUS\\_D\\_ITRS.xls](http://www.itrs.net/Links/2009ITRS/2009Chapters_2009Tables/2009Tables_FOCUS_D_ITRS.xls) (accessed March 2010).
- [29] *Advanced Processes for 193-nm Immersion Lithography*, (Eds: Y. Wei, R. L. Brainard), SPIE, Bellingham, WA, United States of America **2009**, Ch. 10.
- [30] S. Y. Chou, Q. Xia, *Nat. Nanotechnol.* **2008**, 3, 295.
- [31] *CRC Handbook of Chemistry and Physics*, (Eds: D. R. Lide, H. P. R. Frederikse), CRC Press, Inc, **1996**, 12–41
- [32] M. V. Kamalakar, A. K. Raychaudhuri, X. Wei, J. Teng, P. D. Prewett, *Appl. Phys. Lett.* **2009**, 95, 013112.
- [33] B. Yoo, Y. Rheem, W. P. Beyermann, N. Y. Myung, *Nanotechnology* **2006**, 17, 2512.
-